Microwave Engineering
Ulm University

universität ulm

Experimental Study on the Detection of Avalanche Victims using an Airborne Ground Penetrating Synthetic Aperture Radar

Alexander Grathwohl, Philipp Hinz, Ralf Burr, Maximilian Steiner, and Christian Waldschmidt

DOI: 10.1109/RadarConf2147009.2021.9455286

Experimental Study on the Detection of Avalanche Victims using an Airborne Ground Penetrating Synthetic Aperture Radar

Alexander Grathwohl*, Philipp Hinz*, Ralf Burr‡, Maximilian Steiner*, and Christian Waldschmidt*
*Institute of Microwave Engineering, Ulm University, 89081 Ulm, Germany
‡Laboratory for Microtechnology, Ulm University of Applied Sciences, 89081 Ulm, Germany
Email: alexander.grathwohl@uni-ulm.de

***Abstract*—For avalanche victims a short burial time is imperative for a good chance of survival. Although airborne radar systems have been used for a long time in monitoring snow accumulation, their ability to quickly cover large areas of terrain is however not commonly employed in the search for buried victims. The presented method for detection and localization of avalanche victims utilizes a ground penetrating radar mounted on an unmanned aerial system. In order to detect buried victims, the system is operated as a synthetic aperture radar using frequency-modulated continuous-wave modulation. Therefore, it is not dependent on avalanche beacons. This approach is successfully demonstrated in an experimental study, where buried, water-filled mannequin torsos could be detected in fresh as well as compressed mixed snow in a realistic winter environment on 1900 m above mean sea level.**

***Index Terms*—avalanche victims localization, frequency-modulated continuous-wave radar (FMCW), ground penetrating radar (GPR), synthetic aperture radar (SAR), unmanned aerial system (UAS)**

I. Introduction

With the increase in winter tourism in recent decades, recreational winter activities in backcountry also increased. In Switzerland, more than 90 % of the fatalities due to avalanches occur on uncontrolled terrain [1]. Even though the chance of survival has increased in the last years due to improved prevention measures and rescue efficiency, an involvement in an avalanche is still a very serious event. In these events, slab avalanches are the main type of avalanche, and most of the time, accidents occur in dry-snow conditions. The median burial depth for all fully-buried victims is 80 cm.

According to Techel et al. [1], one of the main factors influencing the chance of survival is the burial time. If victims cannot be rescued e.g. by their companions within the first 15 minutes, their survival chance drops rapidly. The median burial time for organized rescue decreased in recent time, but in the decade starting from 2003, it was still as high as 60 minutes. A faster localization of buried avalanche victims would therefore significantly improve the chances of survival.

Although airborne radar systems have been used for decades to map snow accumulation rates [2], their ability to scan large areas of terrain relatively quickly is not commonly used for the detection and localization of avalanche victims. Reference [3] presents a possibility to localize victims with an unmanned aerial vehicle (UAV) but relies on the fact, that victims carry an avalanche beacon. To be able to locate victims even without a beacon, we propose an unmanned aerial system (UAS) equipped with a side-looking frequency-modulated continuous-wave (FMCW) radar operated as a ground-penetrating synthetic-aperture radar (GPSAR). The proposed system, the radar, and its antennas were already presented in [4]–[6].

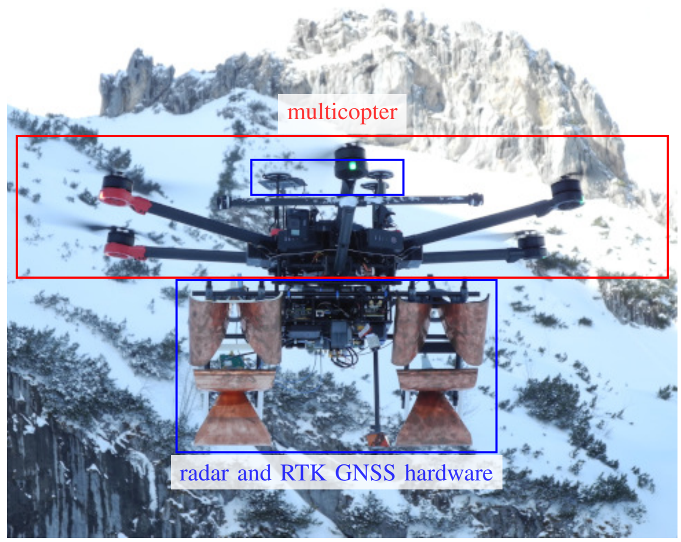

Fig. 1: Multicopter equipped with FMCW SAR and RTK GNSS.

This paper is structured as follows: An overview of the measurement system is presented in Section II. Section III shows how realistic scenarios for the application of the proposed system are recreated. The processing of the collected measurement data is briefly explained in Section IV. Section V presents the measurement results and verifies that the proposed system is able to detect buried objects. Lastly, a conclusion is given in Section VI.

II. Measurement System

The measurement system is displayed in Fig. 1. A multicopter was equipped with a real time kinematic global navigation satellite system (RTK GNSS) and a bistatic FMCW SAR. For this study, the radar was operated in the frequency

(a) Mannequin torso with approximate dimensions 22 cm × 45 cm × 62 cm.

(b) Canister with approximate dimensions 16 cm × 18.5 cm × 24 cm. Its volume is 5 liters.

Fig. 2: Buried objects.

range from 1 GHz to 4 GHz with a transmit power of 15 dBm. The radar achieves a maximum chirp repetition frequency of 110 Hz.

III. Experiment Setup

For a realistic environment, the experiments were conducted in winter at 1900 m above mean sea level near the Alpspitze, Garmisch-Partenkirchen, Germany.

In order to represent avalanche victims in the experiments, plastic mannequin torsos and canisters (see Fig. 2) were filled with water and buried in the snow. Although the dielectric constant of water is frequency- and temperature-dependent, the water-filled containers still realistically represent buried victims. The complex relative permittivity

$$\varepsilon_r = \varepsilon' - \mathrm{j}\varepsilon'' \tag{1}$$

of target objects and their surrounding ground is crucial to understand how a radar detects objects. While ε' is related to the speed of light in the given medium, ε'' is a measure of the losses in that media. A discontinuity in ε' results in diffraction and reflection of signals, which can lead to a detectable signal.

In an avalanche, the mixture of different layers leads to an inhomogeneous ground with varying density, water content and particle size. The real part ε' of the electric permittivity of water in the temperature range of 0 °C to 40 °C is always above 70 [7]. This is sufficiently far away from snow with a low water content and a low density, which has an ε' in the range of 1 to 4 [8]. Water above 0 °C can therefore still represent buried victims for this investigation. If the density of snow is increased due to compression, e.g. in an avalanche, this only has a small effect on ε' [9].

The measurement campaign included two experiments, one conducted in fresh and dry snow and one in a pile of inhomogeneous and compressed snow.

A. Fresh Snow Experiment

In the first experiment, water-filled torsos and canisters were buried. After burying, the top layer above the objects was restored as best as possible.

To simulate air pockets, empty canisters were also buried in the snow. Additionally, corner reflectors were buried and

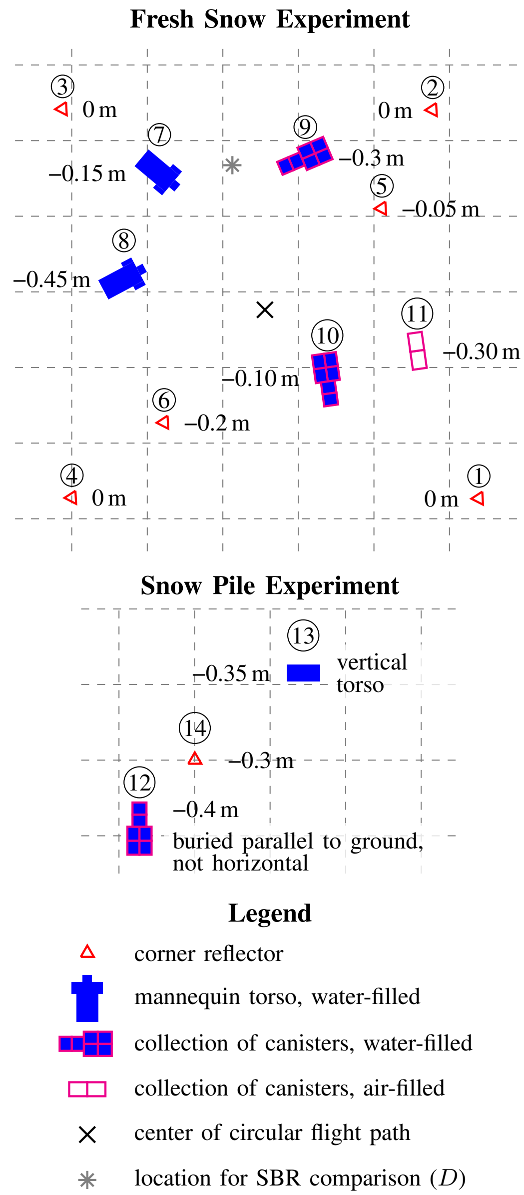

Fig. 3: Experiment layouts. The objects in the map are to scale and displayed on an 1 m × 1 m-grid. For every object its approximate local burial depth is also given. The depth always refers to the object center.

also placed on the surface to mark the measurement area and confirm the correct processing of the data. The ground truth positions of all targets and reflectors were measured using a total station.

The flight trajectory of the drone consisted of circles with a radius of 7.5 m. Data was recorded at six heights in the range from 2 m to 4 m above ground in 0.4 m steps. The drone was automatically controlled and kept a constant velocity of 0.4 $\frac{\mathrm{m}}{\mathrm{s}}$.

Fig. 3 provides a schematic overview of the setup including targets, reflectors, and center of the circular flight path. A photograph of the setup is shown in Fig. 4a.

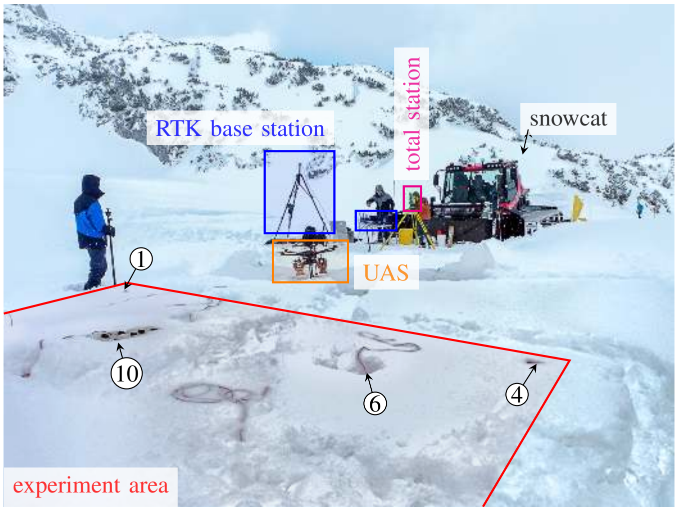

(a) Fresh snow experiment. In the background, the UAS, the RTK base station, the total station, and a snowcat are visible.

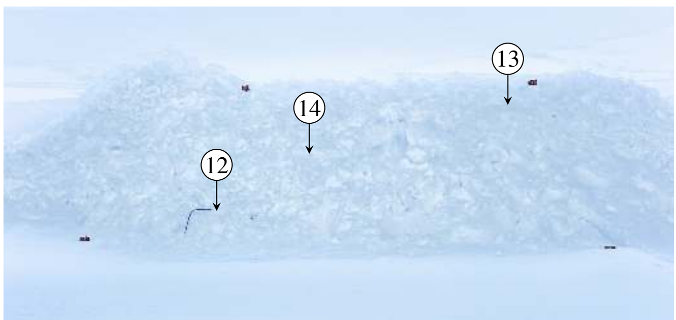

(b) Snow pile experiment.

Fig. 4: Photographs of the experiment setups. The ropes are tied to buried objects to be able to locate them easily afterwards.

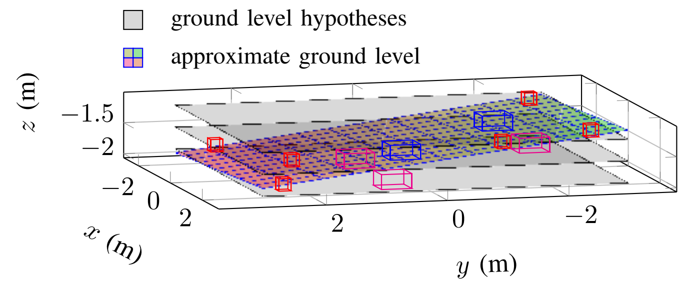

(a) Ground truth target positions, approximate ground level, and ground level hypotheses for the fresh snow experiment.

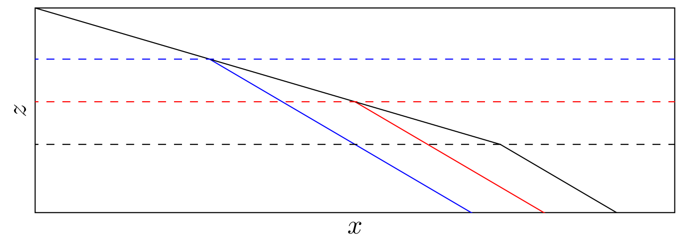

(b) Schematic path (—, —, —) of a signal entering ground at an angle for different ground level hypotheses (- -, - -, - -).

Fig. 5: Focusing with three ground level hypotheses.

TABLE I: Snow profile top to bottom.

layer thickness	layer description
30 cm	Powdery and fresh dry snow, easily penetrable by a fist
18 cm	Small crystals, moist, easily penetrable by four fingers
30 cm	Large crystals, wet, easily penetrable only by a knife blade
10 cm	Large crystals, moist, easily penetrable by a pencil

Lower layers are not relevant for these measurements and are therefore not listed. The total snow height is 188 cm.

To record the snow layers present for this experiment, a survey of the snow profile was done nearby.

B. Snow Pile Experiment

For the second experiment, a snow pile was created with a snowcat. This mixes and compresses the top layers of the snow in the area. In the snow pile a water-filled mannequin torso and canisters were also buried.

Again, the ground truth position was measured using the total station. This time though, the drone was controlled manually. The trajectory coarsely consisted of straight lines at five different heights. Fig. 3 provides a schematic overview of the targets, and Fig. 4b displays a photograph of the setup.

IV. GPSAR Processing

For GPSAR image formation, a backprojection algorithm is used [10]. To be able to focus an image below ground, the ground level and the ε' of the ground need to be known. This is necessary to be able to estimate the electrical path length from any given antenna position to any pixel in the focused image while taking into account the diffraction at the ground level. In the case of these experiments, the ground level is not perfectly horizontal throughout the whole area, see Fig. 5a. Since the implemented GPSAR processing assumes a horizontal plane, processing is run for three different ground levels, while each of these hypotheses are assumed to be perfectly horizontal and flat. Naturally, for each ground level hypothesis, there are areas where this results in a good approximation and areas where the actual ground level is very different.

GPSAR processing was carried out for the relevant range of z-coordinates, so all target positions are included. For the image at a given z-coordinate, there are either one, two, or three different versions to be calculated. This is because images focused above ground do not depend on the ground level, but images below ground differ depending on the chosen ground level hypothesis (see Fig. 5b). For the fresh snow experiment, −1.2 m, −1.55 m, and −1.9 m are used as ground level hypotheses.

Additionally, the flight trajectories of the fresh snow experiment and the snow pile experiment are divided into six and five

TABLE II: Target signal-to-background ratio for single-look and multi-look GPSAR images.

target	object	ground level hypothesis (m)	signal-to-background ratio (dB)						
			single-look aperture height (m)						coherent combination
			2.0	2.4	2.8	3.2	3.6	4.0	
5	corner reflector	−1.20	21.0	19.8	21.3	20.7	22.1	22.3	25.8
6	corner reflector	−1.90	23.5	22.1	22.7	24.3	23.0	23.6	28.6
7	water-filled torso	−1.20	21.6	23.4	24.4	24.7	25.7	23.1	29.7
8	water-filled torso	−1.55	23.3	22.4	21.3	21.5	21.5	22.4	22.8
9	water-filled canisters	−1.20	21.6	20.9	22.1	21.4	22.9	20.9	26.1
10	water-filled canisters	−1.55	28.0	26.9	23.2	23.0	23.0	22.2	28.8
11	air-filled canisters	−1.55	22.0	21.8	22.4	20.8	21.0	21.3	21.2
D	nothing	−1.20	21.0	19.8	21.7	21.1	22.1	21.3	21.4

apertures, respectively. This way each aperture corresponds to a partial trajectory with approximately constant height and velocity. The resulting GPSAR images for the apertures were coherently combined into a multilook image, i.e. the complex-valued images were added.

A constant false alarm rate (CFAR) algorithm was applied to detect targets for every combined image. By merging all CFAR detection images, a single global detection image was formed as the result.

V. Measurement Results

The survey of the snow profile revealed a total snow height of 188 cm over the solid ground. Table I lists the top layers relevant to this experiment and their properties. All layers below the ones listed consisted of wet snow due to intense rain in the weeks before the experiment.

A. Fresh Snow Experiment

For this evaluation the real part of the permittivity of the snow is assumed to be $\varepsilon' \approx 2$, since the relevant top layer consisted of fresh snow with very fine crystals and low water content [8].

Table II lists the signal-to-background ratio (SBR) for all buried targets for the images obtained from single apertures (see Section IV) as well as for the multilook images obtained by their coherent combination. To calculate the signal power of a target, first the pixel of maximum power is located in an area around the known ground truth target position. The total power in a 3×3-grid of pixels centered on that maximum is then used. A histogram analysis of the power in all pixels is used to calculate the background level. It is estimated as the value where the distribution reaches its maximum.

The values for each target are calculated for the ground level hypothesis that best fits the target location. For comparison, a location D with no buried target is also investigated (see Fig. 3). Due to clutter, any local maximum near D will result in an SBR significantly greater than zero. As a rough measure of the detectability of a target, the difference between the SBR values of this target and D can be used.

For targets 5–7 and 9, the coherent combination leads to a significant increase in SBR and improves the detectability of the targets. For targets 8 and 10, the SBR differs between apertures. This is likely because multiple scattering centers of the objects are best visible from different angles. The SBR does not increase for the multilook image here, since the scattering centers are not spatially aligned in the images. Because the effects due to clutter are different for the apertures, the SBR of D stays approximately constant.

Comparing the SBRs of the targets and D reveals, that targets 5 to 7 and 9 to 10 should be easily detectable in the multilook image. It also shows that there is no significant response from the empty canisters. This is due to the very small difference between the electric permittivities of dry snow and air. This also explains, why none of the pathways needed to setup the experiment are visible in the detection image, although they are clearly visible in Fig. 4a.

One of the buried torsos (target 8) is difficult to distinguish from clutter. This is likely due to the wet snow layers in the same depth.

Additionally, it can be concluded, that the coherent combination of images from multiple apertures is necessary for the detection of buried objects with the proposed system.

The three-dimensional CFAR detection image is generated from multilook data as described in Section IV and is shown in Fig. 6a. All corner reflectors are clearly visible in this detection image. Additionally, the two collections of water-filled canisters are successfully detected. This also applies to target 7, which is a water-filled, shallowly-buried mannequin torso.

The other water-filled torso is still visible, but, as anticipated, the response a lot weaker than for the other targets. As expected, the empty canisters are not visible in the detection image.

B. Snow Pile Experiment

For this evaluation the real part of the permittivity of the snow is unknown, since the snow pile consisted of a mix of the top few layers of the snow profile. It included layers with higher water content and was mixed and compressed when the pile was created. Although the permittivity of the snow in the pile is inhomogeneous, it is necessary to assume a constant value for this evaluation. Here, $\varepsilon' = 4$ was used for image focusing.

The three-dimensional resulting CFAR image for the snow pile experiment is shown in Fig. 6b. Although the pile surface is a lot more steep in comparison to the first experiment, the corner reflector (target 14) is clearly visible. This shows again that a focusing of the targets is possible. The water-filled canisters are easily detected in this inhomogeneous and

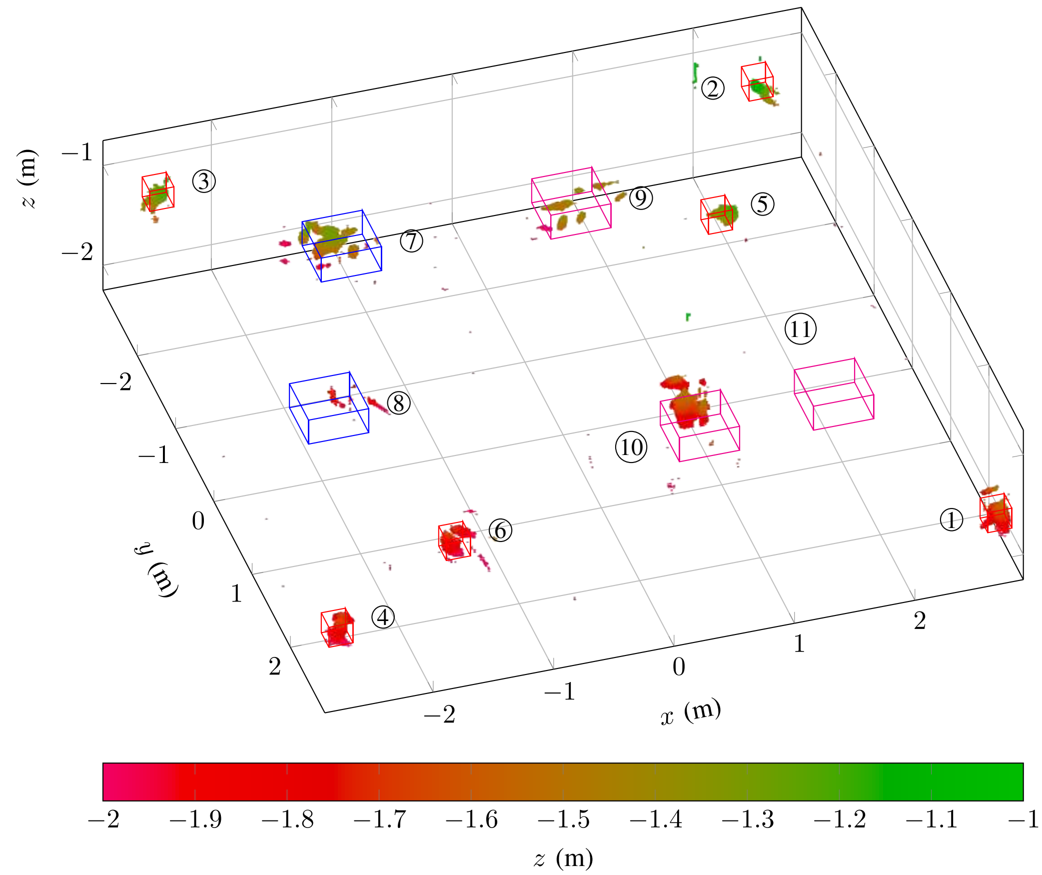

(a) Fresh snow experiment. The coordinate system (x, y) is centered on the center of the flight path.

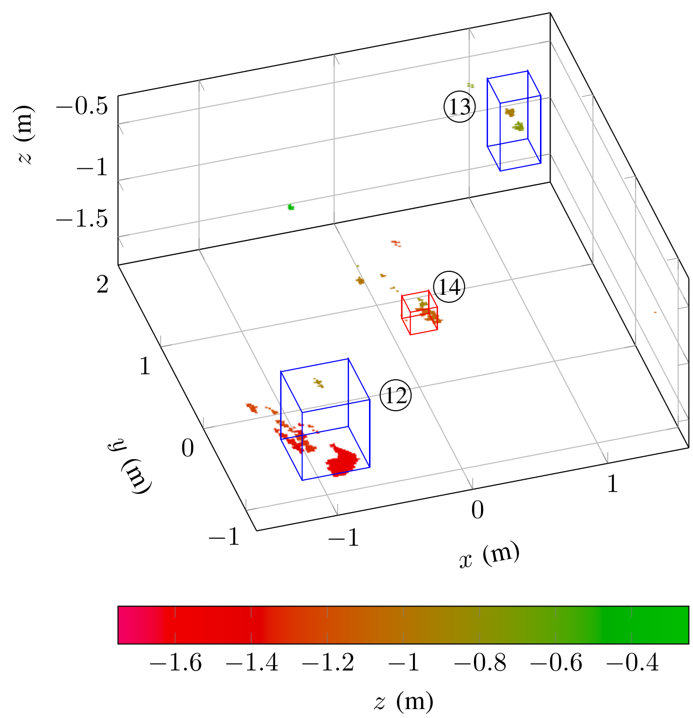

(b) Snow pile experiment. The coordinate system (x, y) is centered on the experiment area's center.

Fig. 6: Three-dimensional CFAR detection images for both experiments. Ground truth positions and size of buried targets are displayed with colored boxes.

compressed snow. The response of the torso is weaker than the response of the canisters, but it is still detected.

The canisters and torsos were buried at a maximum depth of 40 cm below the surface. Although the median burial depth of avalanche victims is more than that, this experiment included inhomogeneous and compressed snow with higher water content. A low water content in the snow would result in lower signal loss and a greater difference between the permittivities of the targets and the surrounding snow layers. This increases the maximum depth an object can be detected. For the more common slab avalanches with very dry snow, the detection and localization of avalanche victims with deeper burial depths is therefore likely possible.

VI. Conclusion

In this work, an airborne UAS with a GPSAR was proposed for the detection and localization of avalanche victims. It was shown that shallowly buried victims can be detected in dry snow typical of most avalanche incidents. This is true even if the snow is inhomogeneous and compressed. Coherently combining images from multiple apertures improves the SBR of the targets and is necessary for a reliable detection. This detection is robust against air pockets and pathways in the snow.

By implementing the signal processing in a real-time manner on the drone hardware, the detection of victims would be possible even during flight. Systems like this could support avalanche victim localization and increase their survival chance.

Acknowledgment

The authors would like to thank the BAYERISCHE ZUGSPITZBAHN Bergbahn AG for making this measurement campaign possible.

References

[1] F. Techel and B. Zweifel, "Recreational avalanche accidents in switzerland: Trends and patterns with an emphasis on burial, rescue methods and avalanche danger," in *International Snow Science Workshop (ISSW)*, Oct. 2013.

[2] HP. Marshall, M. Robertson, M. Mason, C. Rodriguez, and T. Meehan, "Radar remote sensing of mountain snow: a review of current ground-based, airborne and satellite-based approaches to monitoring snow properties," in *International Snow Science Workshop (ISSW)*, Oct. 2018.

[3] M. Silvagni, A. Tonoli, E. Zenerino, and M. Chiaberge, "Multipurpose UAV for search and rescue operations in mountain avalanche events," *Geomatics, Natural Hazards and Risk*, vol. 8, no. 1, pp. 18–33, Oct. 2016.

[4] M. Schartel, R. Burr, W. Mayer, N. Docci, and C. Waldschmidt, "UAV-based ground penetrating synthetic aperture radar," in *IEEE MTT-S International Conference on Microwaves for Intelligent Mobility (ICMIM)*, Apr. 2018.

[5] R. Burr, M. Schartel, P. Schmidt, W. Mayer, T. Walter, and C. Waldschmidt, "Design and implementation of a FMCW GPR for UAV-based mine detection," in *IEEE MTT-S International Conference on Microwaves for Intelligent Mobility (ICMIM)*, Apr. 2018.

[6] R. Burr, M. Schartel, W. Mayer, T. Walter, and C. Waldschmidt, "Lightweight broadband antennas for UAV based GPR sensors," in *15th European Radar Conference (EuRAD)*, Sept. 2018.

[7] T. Meissner and F. J. Wentz, "The complex dielectric constant of pure and sea water from microwave satellite observations," *IEEE Transactions on Geoscience and Remote Sensing*, vol. 42, no. 9, pp. 1836–1849, Sept. 2004.

[8] TH. Achammer and A. Denoth, "Snow dielectric properties: from DC to microwave X-band," *Annals of Glaciology*, vol. 19, pp. 92–96, 1994.

[9] S. Sugiyama, H. Enomoto, S. Fujita, K. Fukui, F. Nakazawa, and P. Holmlund, "Dielectric permittivity of snow measured along the route traversed in the japanese–swedish antarctic expedition 2007/08," *Annals of Glaciology*, vol. 51, no. 55, pp. 9–15, 2010.

[10] M. Schartel, K. Prakasan, P. Hügler, R. Burr, W. Mayer, and C. Waldschmidt, "A multicopter-based focusing method for ground penetrating synthetic aperture radars," in *IEEE International Geoscience and Remote Sensing Symposium (IGARSS)*, Jul. 2018.